J. Fluid Mech. (1996), *vol.* 316, *pp.* 1–27

Axis switching and spreading of an asymmetric jet: the role of coherent structure dynamics

By K. B. M. Q. ZAMAN
NASA Lewis Research Center, Cleveland, OH 44135, USA

(Received 1 August 1994 and in revised form 4 December 1995)

The effects of vortex generators and periodic excitation on vorticity dynamics and the phenomenon of axis switching in a free asymmetric jet are studied experimentally. Most of the data reported are for a 3:1 rectangular jet at a Reynolds number of 450000 and a Mach number of 0.31. The vortex generators are in the form of 'delta tabs', triangular-shaped protrusions into the flow, placed at the nozzle exit. With suitable placement of the tabs, axis switching could be either stopped or augmented. Two mechanisms are identified governing the phenomenon. One, as described by previous researchers, is due to the difference in induced velocities for different segments of a rolled-up azimuthal vortical structure. The other is due to the induced velocities of streamwise vortex pairs in the flow. While the former mechanism, referred to here as the ω_θ-*dynamics*, is responsible for a rapid axis switching in periodically forced jets, e.g. screeching supersonic jets, the effect of the tabs is governed mainly by the latter mechanism, referred to as the ω_x-*dynamics*. Both dynamics can be active in a natural asymmetric jet; the tendency for axis switching caused by the ω_θ-dynamics may be, depending on the streamwise vorticity distribution, either resisted or enhanced by the ω_x-dynamics. While this simple framework qualitatively explains the various observations made on axis switching, mechanisms actually in play may be much more complex. The two dynamics are not independent as the flow field is replete with both azimuthal and streamwise vortical structures which continually interact. Phase-averaged measurements for a periodically forced case, over a volume of the flow field, are carried out in an effort to gain insight into the dynamics of these vortical structures. The results are used to examine such processes as the reorientation of the azimuthal vortices, the resultant evolution of streamwise vortex pairs, as well as the redistribution of streamwise vortices originating from secondary flow within the nozzle.

1. Introduction

In a continuing effort to increase mixing in free shear flows, various methods of flow control are being explored in an experimental research program at NASA Lewis Research Center. The effect of passive, vortex-generating 'tabs' has been explored over the past several years (Ahuja & Brown 1989; Zaman, Reeder & Samimy 1994). Tabs are protrusions into the flow placed at the jet-nozzle exit. They produce large distortions in the jet which are accompanied by a significant increase in entrainment and spreading. While experimenting with asymmetric jets, it was observed that the tabs could not only affect mixing but also the phenomenon of axis switching in these jets. Depending on the number and placement, the tabs could either stop or promote the axis switching. These observations led to a further detailed investigation.

Axis switching is a phenomenon in which the cross-section of an asymmetric jet

evolves in such a manner that, after a certain distance from the nozzle, the major and the minor axes are interchanged. Most previous studies involving rectangular or elliptic jets reported axis switching (e.g. Sforza, Steiger & Trentacoste 1966; Sfeir 1978; Krothapalli, Baganoff & Karamcheti 1981). From available data (e.g. Tsuchiya, Harikoshi & Sato 1986; Ho & Gutmark 1987), it becomes apparent that the switching is not due to a helical turning of the jet column. Instead, the jet cross-section expands in the direction of the minor axis and contracts in the direction of the major axis, and thereby a 90° switch takes place after a certain downstream distance. Typically, a first switchover is quite prominent and may take place a few equivalent diameters from the nozzle exit. A second, occurring much farther downstream, and even a third switchover have been observed (Hussain & Husain 1989); the latter switchovers are usually faint, however, and may not be easily detectable.

Often the location of the switchover may be quite uncertain. Krothapalli *et al.* (1981) compared their data on rectangular jets with previous results and showed that the distance of the first switchover from the nozzle increased with increasing aspect ratio of the nozzle. However, the uncertainty range was large; for example, the switchover location for a 10:1 aspect ratio jet was within a range of $x/D = 25$ to 65, and that for a 3:1 aspect ratio jet could be anywhere from very close to the nozzle to as far downstream as $x/D = 40$. Here, D denotes the equivalent diameter based on the nozzle exit area. Part of the uncertainty in the data could be due to the different methods employed in the previous experiments to determine the switchover, e.g. flow visualization and various forms of flow field surveys. However, it becomes apparent that the switchover location could also be affected by other factors, e.g. jet initial condition, compressibility, etc.

In fact, even whether a switchover will occur or not with a given nozzle may be uncertain and depend on the flow condition. This is illustrated by the data in figure 1, taken in connection with a study of comparative jet spreading with various asymmetric nozzles. The data are obtained by Pitot probe surveys for a small 3:1 rectangular nozzle with $D = 1.47$ cm. Figures 1(*a*) and 1(*b*) show that by $x/D = 14$ the jet cross-section, at a subsonic condition, has become round and it stays that way farther downstream. There might be some mild undulations in the variations of the major and the minor axes but this is not significant. What is significant, and rather puzzling, is the fact that the same nozzle when run at a supersonic condition exhibits a clear axis switchover. This is illustrated in figures 1(*c*) and 1(*d*). Note that the nozzle major axis is aligned vertically as sketched in these figures. A clearer axis switchover at supersonic conditions was also observed with a 3:1 elliptic nozzle as well as a 4:1 and a 8:1 rectangular nozzle (Zaman 1994). The data of figure 1 will be further discussed in the text.

Gutmark & Schadow (1987) had reported an interesting set of data on the flow from small aspect ratio slot nozzles. When the nozzle was essentially an orifice, the jet went through a rapid axis switchover by $x/D = 2$. However, when a contraction section leading to the nozzle exit was added, the resulting jet diverged in the major axis plane over the measurement range of $x/D = 10$. Such a trend corroborates an earlier observation that the axis switchover occurs '... further downstream for a jet exiting from a long channel than for a jet exiting from an orifice' (Krothapalli *et al.* 1981). Hussain & Husain (1989) further confirmed this difference between jets from an orifice nozzle and a nozzle with contraction.

These observations raise the question of what determines the various trends. Why is there axis switching in the supersonic condition of figure 1 but none in the subsonic condition? Why does the axis switching observed with an orifice nozzle stop when a

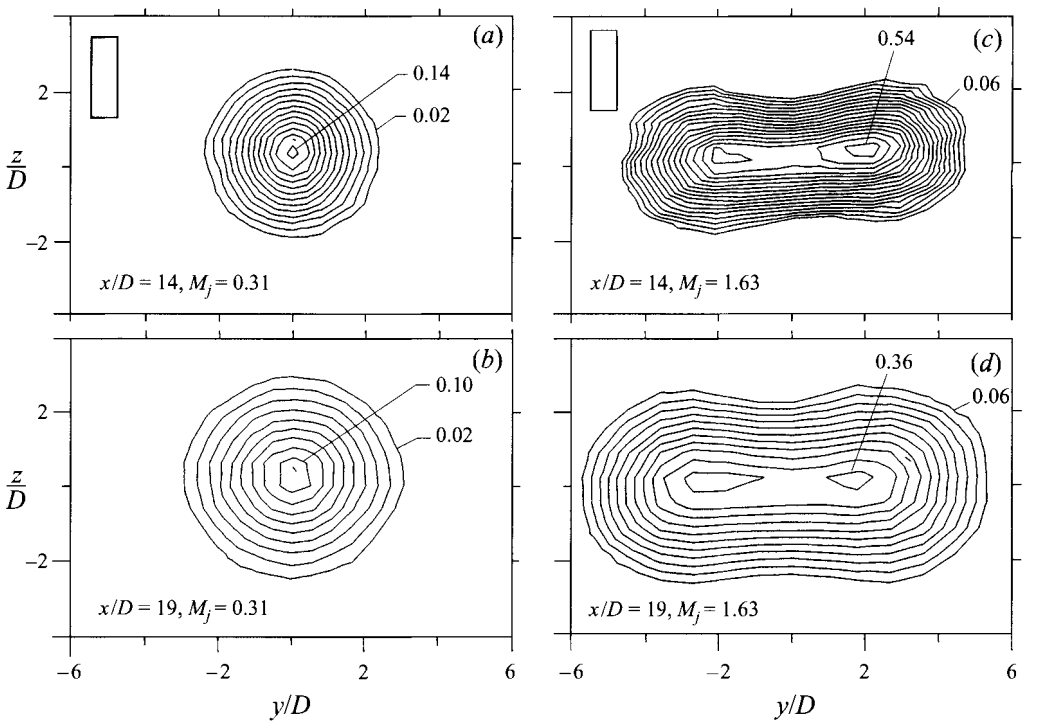

FIGURE 1. Mach number contours for a 3:1 rectangular jet (D = 1.47 cm) at indicated streamwise locations (x/D) and jet Mach numbers (M_j). The normalized mass flux ($\dot{m}/\dot{m}_e$, $\dot{m}_e$ being initial flux) for the four cases are: (*a*) 4.42, (*b*) 5.71, (*c*) 4.01, and (*d*) 5.40.

contraction section is added? These questions, as well as the profound effect of the tabs on axis switching, to be discussed shortly, provided the motivation for carrying out the present study.

An explanation for axis switching in a jet has been given by Hussain & Husain (1989). This explanation is based on the dynamics of rolled-up azimuthal vortex structures (see also Ho & Gutmark 1987; Toyoda, Shirahama & Kotani 1991; Hertzberg & Ho 1992; Kambe & Takao 1971; Viets & Sforza 1972; Dhanak & Bernardinis 1981; Kiya, Ishii & Kitamura 1991). This will be reviewed in the text. It will be reasoned that while this 'ω_θ-dynamics' explains many of the observations, including the one made for the supersonic case, the effects of the tabs are not explained satisfactorily. The dynamics of streamwise vortex pairs occurring in an asymmetric jet, referred to as the 'ω_x-dynamics', are inferred to also play a significant role. The important role of streamwise vortices in the entrainment process of an axisymmetric jet was convincingly demonstrated by Liepmann & Gharib (1992). Here, it is found that the ω_x-dynamics also quite elegantly explain the effect of the tabs on the axis switching phenomenon. The main objective of the present paper is to discuss the relevant results and elucidate these inferences.

It should be apparent that the ω_x- and the ω_θ-dynamics are not independent of each other. The distortion of the azimuthal vortex structures can lead to streamwise vortices even in the time-averaged flow field, as demonstrated, for example, by the computational results of Grinstein, Gutmark & Parr (1994). A set of experiments has been conducted in an attempt to shed light onto these processes. Periodic forcing, via plenum chamber resonance, has been used to organize the azimuthal vortex structures. The method of phase averaging has been employed to investigate the vorticity field in

extensive detail for a specific case of the excitation. The results illustrate such details of the flow field as the reorientation of the azimuthal vortex rings, their time variation, the nature and time variation of the streamwise vortex pairs, etc. These results are also discussed in this paper.

2. Experimental method

The study was conducted with a 3:1 rectangular nozzle having an equivalent diameter, $D = 6.35$ cm. The essential features of the flow facility are shown schematically in figure 2. The nozzle contracted from a 41 cm round section to the 9.75 cm × 3.25 cm rectangular section within a length of 23 cm, the transition of the geometry starting at 12.7 cm from the exit. Compressed air was supplied through the other end of the plenum chamber and the flow discharged into the ambient. The plenum chamber had acoustic suppressor and flow conditioning units, and the turbulence intensity at the jet exit centre was approximately 0.15%. The nozzle exit boundary layer was measured at several peripheral locations. The momentum thickness over most of the two long edges was approximately $\theta/D = 0.004$. On the short edges and near the corners, deviations by as much as 25% occurred. From the shape factor the boundary layer was inferred to be nominally laminar everywhere. Here, it should be mentioned that flow separation at the cusped joints in the facility (figure 2*a*) might be expected to produce some unsteadiness. This together with the flow geometry in that region could support Taylor–Görtler instability, which would generate streamwise vorticity. However, such an effect should be small, as spot checks with a circular nozzle showed uniform boundary layer thickness on the periphery (Raman, Zaman & Rice 1989). With the rectangular nozzle, the most significant source of streamwise vorticity is secondary flow within the nozzle, and this is further discussed in §3.1.

Hot-wire measurements were carried out for a jet Mach number $M_j = 0.31$ which corresponded to a Reynolds number $Re_D \approx 450000$. The flow field measurement technique was an extension of the method described by Zaman *et al.* (1994). Two X-wire probes, one in the u-v and the other in the u-w configuration, were traversed successively through the same grid points. The two probes were located at the same z location and separated in y by 2.54 cm. The step size in y was chosen to be a submultiple of the separation distance so that a shift of the w-array by an integral number of steps matched the corresponding v-array. The distributions of v and w in the y- and z-directions yielded ω_x. Gradient correction was applied to all v and w data with a procedure similar to that used by Bell & Mehta (1992).

For all data sets, the hot wires were calibrated at the start and the calibration was spot checked at the end of the run. For calibration, the two X-probes were placed at the nozzle exit (tabs removed) centred around the axis. The constant-temperature anemometer outputs from the four sensors were least-squares fitted with fourth-order polynomials as a function of the jet velocity which was obtained via measurement of the nozzle pressure ratio and isentropic flow calculations. The polynomial coefficients were later used to calculate the velocities using cosine laws. The jet exit velocity (U_j) was constantly monitored during data acquisition. The data acquisition was stopped if U_j deviated beyond $\pm 1.5\%$; data normalization was done by the updated value of U_j. The probe traverses and data acquisition were done by automated computer (Micro-Vax) control. The (Klinger) probe traverser had a resolution of 0.0025 cm.

The effect of the measurement grid size on the convergence of ω_x was tested. With the centre of the grid coincident with the vortex centre (determined by preliminary measurement), the grid size was progressively reduced while measuring ω_x by line

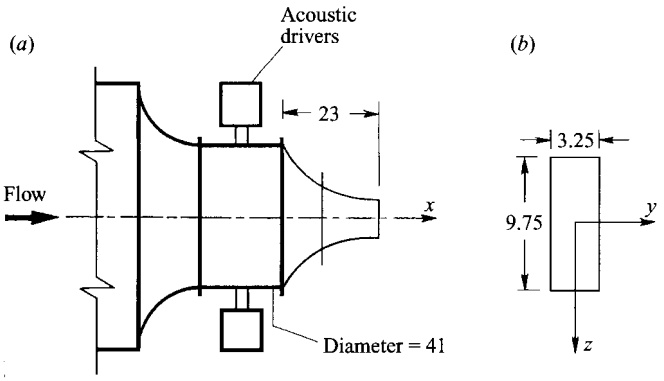

FIGURE 2. Schematic of jet facility: (*a*) side view of the exit section, (*b*) exit geometry of the rectangular nozzle. Dimensions are in cm.

integration of v and w. Sufficiently small grid size, to yield invariant ω_x-amplitude, was thus chosen for each x-station and used in the subsequent data acquisition. Inside the core of the jet, the uncertainty in the normalized streamwise velocity component was estimated to be within $\pm 1\%$, and that in the mean streamwise vorticity to be approximately $\pm 20\%$; similar uncertainties were reported for past measurements (Hussain & Zaman 1980; Quinn 1992). However, progressively larger uncertainties and errors are expected away from the core owing to flow angularity, turbulence, and small density and temperature fluctuations at the jet Mach number under consideration. On the edges of the flow field especially, the hot-wire data are contaminated by occasional flow reversal. The data shown are as measured, and no correction is attempted. Thus, the overall vorticity distributions should be considered as qualitative. It should also be mentioned here that whereas ω_x was obtained from the actual spatial distributions of $v(y,z)$ and $w(y,z)$, Taylor's hypothesis was invoked to estimate the components ω_y and ω_z. The procedure for this, and the errors, will be discussed in §3.3.

The vortex generators used were the 'delta tabs' (Zaman *et al.* 1994). Each had a triangular shape with the base placed on the nozzle wall and the apex leaning downstream at an angle of 45°. The width of the tab at the base was 1.8 cm and the area blockage due to each was approximately 1.8% of the nozzle exit area.

An (Altec Lansing) acoustic driver was used for the excitation studies. The excitation was imparted in the form of a 'plane wave' perturbation at the nozzle exit. The choice of the excitation frequency (f_p) was dictated by the plenum chamber resonances. Based on the studies of Hussain & Husain (1989), which showed a large effect between Strouhal numbers ($St = f_p D/U_j$) of 0.45 and 0.85, a resonance of $f_p = 1.01$ kHz was chosen. This corresponded to $St = 0.6$; the maximum available amplitude of $u'_{fe}/U_j = 0.004$ was used, where u'_{fe} is the r.m.s. fundamental measured at the jet exit centre.

The excitation signal was used as the reference for the phase averaging. A survey was conducted first and a subharmonic in the velocity spectra was noted to develop for $x/D > 1.0$. From the survey of the velocity spectra, to be discussed further with the phase-averaged data, $x/D = 2.2$ was chosen as the downstream limit for the measurements. Upstream of this station, the subharmonic was deemed minimal and not to affect the phase-average measurements. From probe resolution considerations, on the other hand, the upstream limit for the measurements was set at $x/D = 0.85$. The time-averaged data, however, were obtained over the range $0.5 < x/D < 20$. The phase-averaged data were acquired on-line for 19 phase points over a complete period of the

fundamental. The convergence of the phase-averaged data was tested initially, the data presented are typically averages over approximately 200 cycles. In the following, the notation $\langle f \rangle$ is used to indicate phase-average of a function f.

3. Results

3.1. *Effect of tabs and excitation on axis switching*

Figure 3 shows the streamwise variations of the jet half-velocity width measured on the major and the minor axis planes of the nozzle; B represents the distance between the points where the velocity is half of the local centreline velocity. One finds that within the x-range covered, the jet without any tabs has not gone through an axis switching (figure 3*a*). Two delta tabs placed on the narrow edges of the nozzle have caused a rapid switchover by $x/D = 2.5$ (figure 3*b*). In comparison, two delta tabs placed on the long edges have caused the jet to continue to diverge on the major axis plane within the measurement range (figure 3*c*). Figure 3(*d*) shows data obtained for the case of artificial excitation. Clearly, the excitation has also drastically affected the jet spreading in the minor and the major axis planes.

Data showing the time-averaged evolution of the flow fields corresponding to the four cases of figure 3(*a–d*) are presented in figure 4(*a–d*). Contours of longitudinal velocity are shown in the left column while the streamwise vorticity contours are shown in the right column, for the indicated x/D locations. Figure 4(*a*) shows that the undisturbed jet cross-section has become essentially round by $x/D = 16$, and that the axes have not switched within this distance. Similar behaviour was observed in figures 1(*a*) and 1(*b*) with the smaller, but geometrically similar, nozzle. It is also clear from figure 4(*a*) that streamwise vortices are present in the flow even without any tabs. One vortex originating from each corner of the nozzle dominates the flow field. The vortices are seen to lose their strength with increasing downstream distance and by $x/D = 16$ the amplitudes are below the measurement noise level.

Shortly downstream of the nozzle, the four vortices in the case of figure 4(*a*) form two counter-rotating pairs, one on each end of the major axis. The sense of rotation, shown by the arrows with the data for $x/D = 1$, is such that there is an ejection of jet core fluid by each pair. That is, the fluid in between the two vortices of a pair is forced out into the ambient region. For ease of identification, such a vortex pair will be referred to in the following as the *outflow* pair, and conversely, an *inflow* pair will be of the opposite sense. Such a notation identifies the vortex pairs uniquely and the sense remains unchanged even under a different coordinate system. The influence of these vortex pairs on the flow field is discussed in §3.2.

Here, it is instructive to examine similar time-averaged vorticity results obtained by a few other investigators in comparable flows (Quinn 1992; Davis & Gessner 1992; Miau *et al.* 1990). Quinn reported data for a square nozzle. Pairs of counter-rotating streamwise vortices originated from each of the four corners of the nozzle. Thus, the flow field of the square jet was characterized by eight streamwise vortices instead of the four seen in the rectangular case (figure 4*a*). Shortly downstream of the nozzle, two adjacent vortices on a side of the square cross-section moved closer to each other to form an outflow pair. By $x/D = 1.25$, the two axes of the jet cross-section interchanged position with the two diagonals, i.e. turned by 45°. Farther downstream, for $x/D > 5$, the jet cross-section became effectively round. The 45° switching of axes in a square jet will be addressed further in the following.

Davis & Gessner (1992) made measurements in a duct transitioning from a circular to rectangular cross-section. At the end of the rectangular section, their data showed

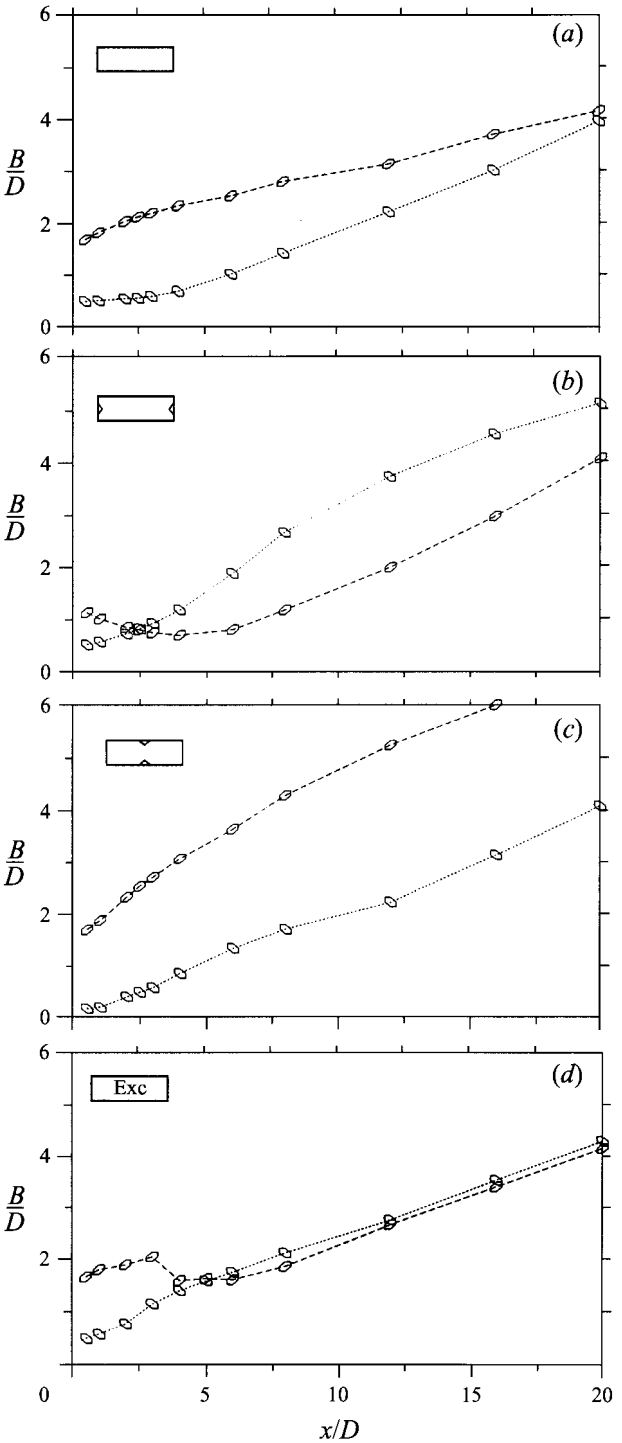

FIGURE 3. Streamwise variations of jet half-velocity-width; ∞, minor axis plane, ∘, major axis plane. (*a*) no tab, (*b*) two tabs on ends, (*c*) two tabs on sides, and (*d*) acoustic excitation at $St = 0.6$ and $u'_{fe}/U_j = 0.004$.

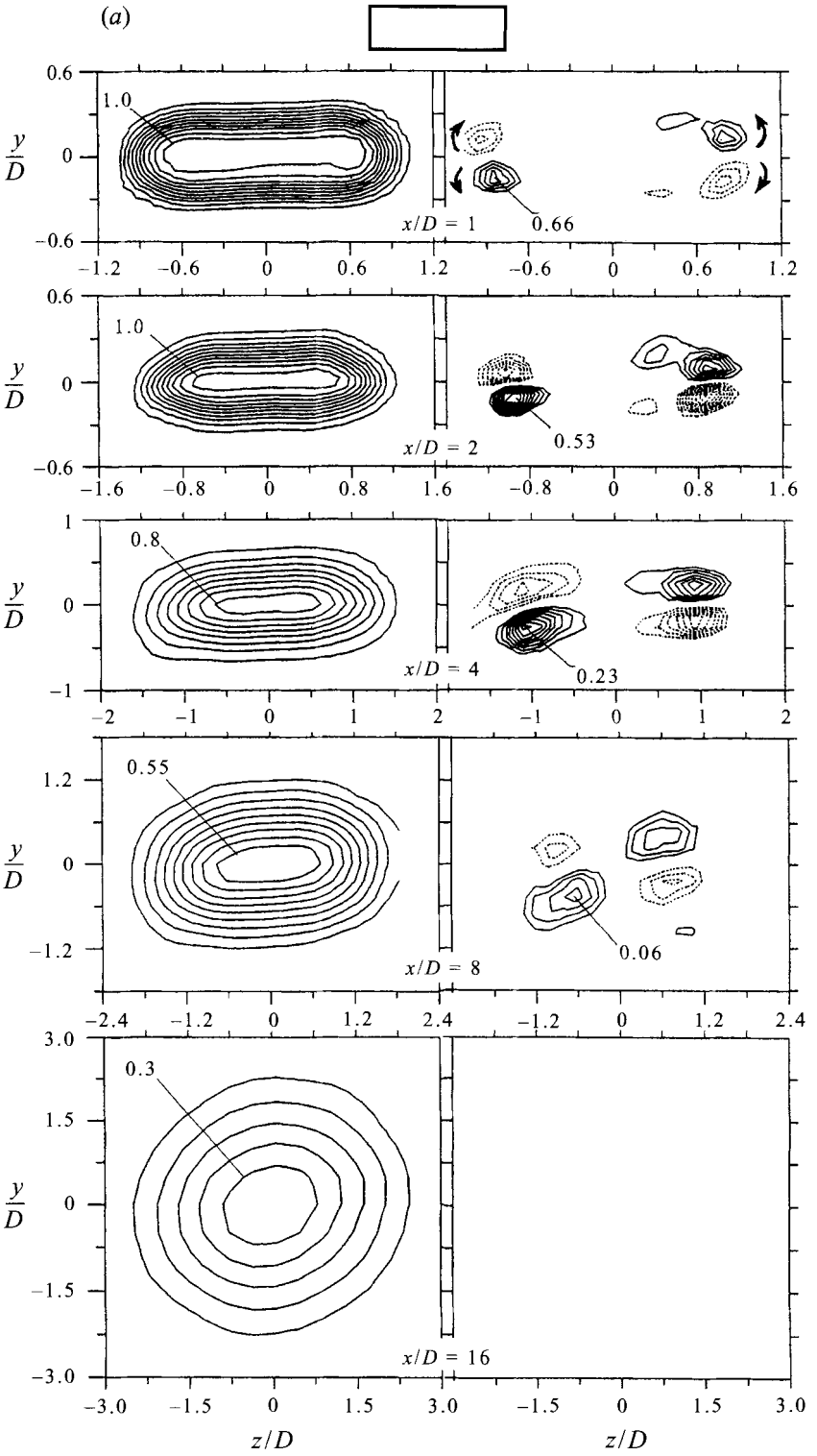

FIGURE 4(*a*). For caption see page 11.

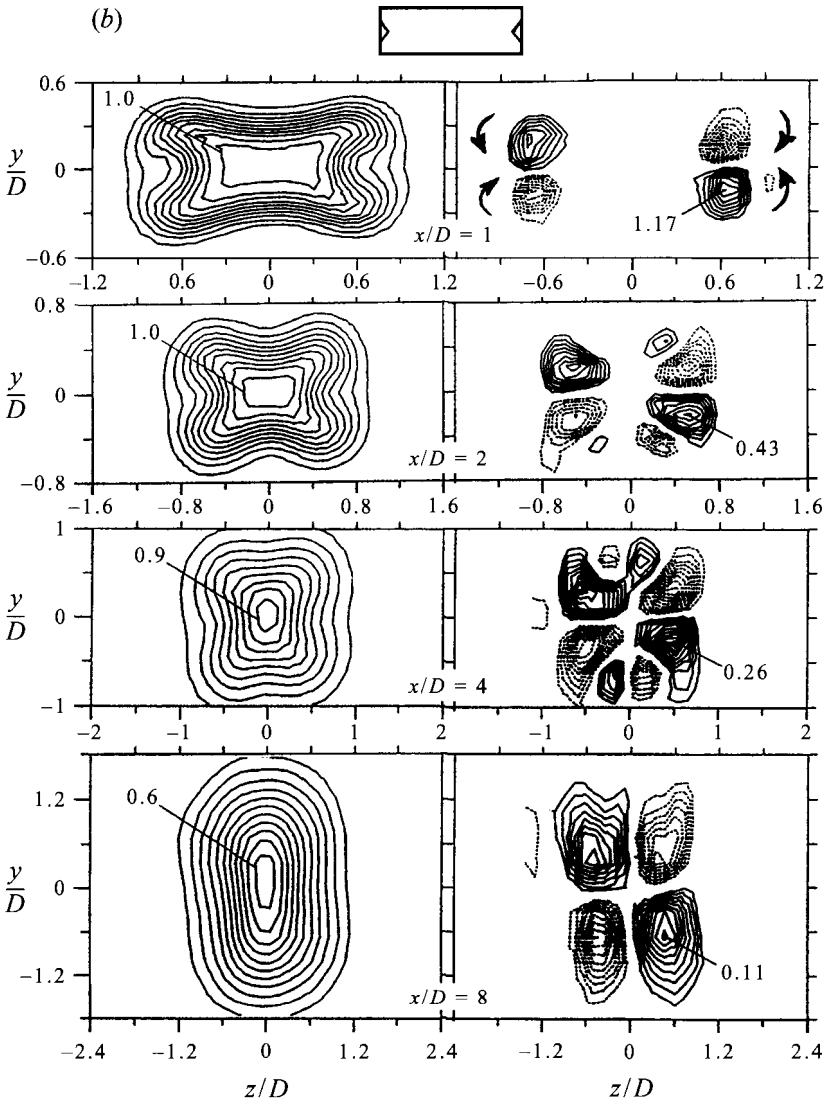

FIGURE 4(*b*). For caption see page 11.

the presence of four streamwise vortices. The distribution was quite similar to that measured in the present case, except that the sense of rotation was opposite, i.e. the two pairs formed at the ends of the major axis were of the inflow type. A subsequent computational study corroborated well these experimental results (Sotiropoulos & Patel 1993). The other experiment, of Miau *et al.* (1990), also involved a duct transitioning from circular to rectangular section. There were only minor differences in the duct geometries. For example, the cross-sectional area was held constant in the latter experiment while that in Davis & Gessner's enlarged by 15% before reducing back to the inlet value. These differences, however, resulted in streamwise vorticity distribution in Miau *et al.*'s experiment with a sense opposite to that in Davis & Gessner's.

A primary source of streamwise vorticity in the flow through a transitioning duct is Prandtl's first kind of secondary flow, i.e. lateral pressure gradients skewing the

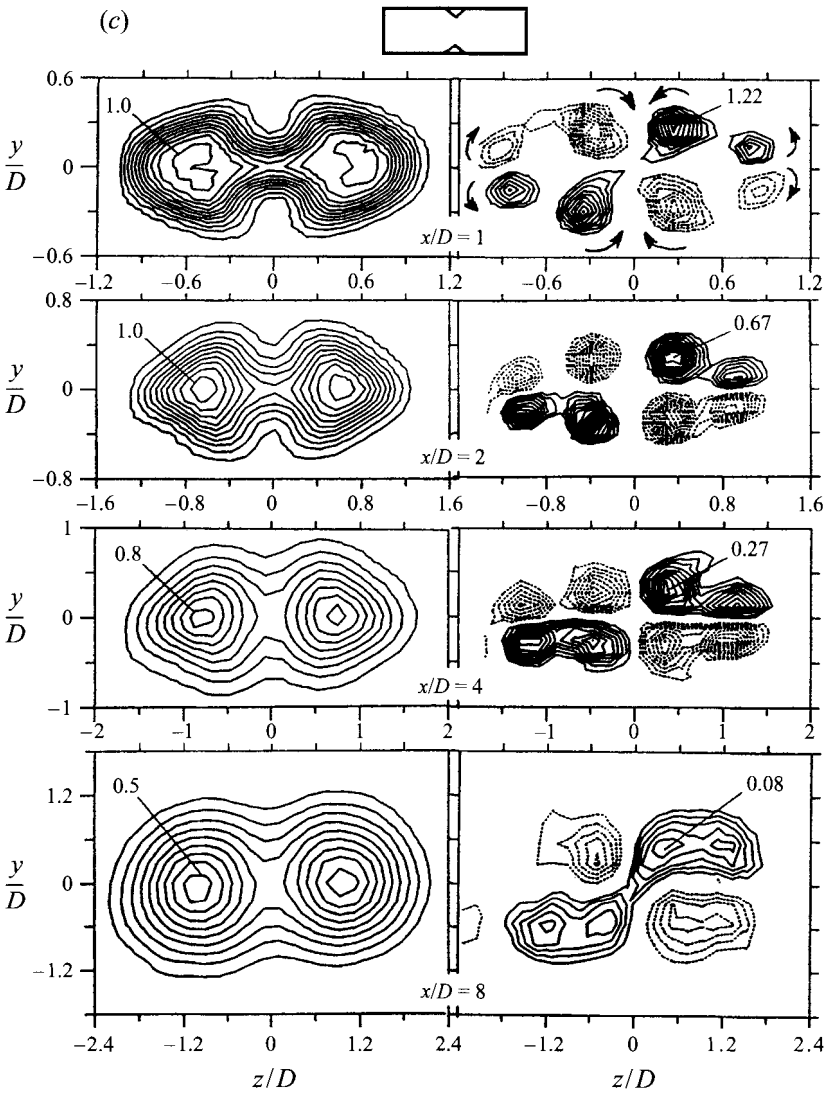

FIGURE 4(c). For caption see facing page.

boundary layer on the duct inner walls (Bradshaw 1987). The flow is accelerated differently along different sections of the duct wall which gives rise to the lateral pressure gradients. While the experiments of Davis & Gessner and of Miau *et al.* dealt with transitioning ducts with only minor variations in the cross-sectional area, a jet nozzle involves large contradiction ratios. For example, the contraction ratio with the present nozzle is over 40 (figure 2). As far as the sense of the streamwise vortices is concerned, it appears, from a consideration of the expected pressure gradients, that the outflow pairs should be the common ones in flows from convergent asymmetric nozzles. (Indeed, author's experiments with certain other asymmetric nozzles also yielded the outflow pairs. Also, the upstream secondary flow may be expected to generate a total of eight, or four pairs of, streamwise vortices in the rectangular nozzle. However, the lateral pressure gradient developed on the approach to the long sides of the nozzle are more intense than that developed on the short sides. Thus, four of the eight vortices dominate the flow. With symmetry, obviously, all eight vortices emerge

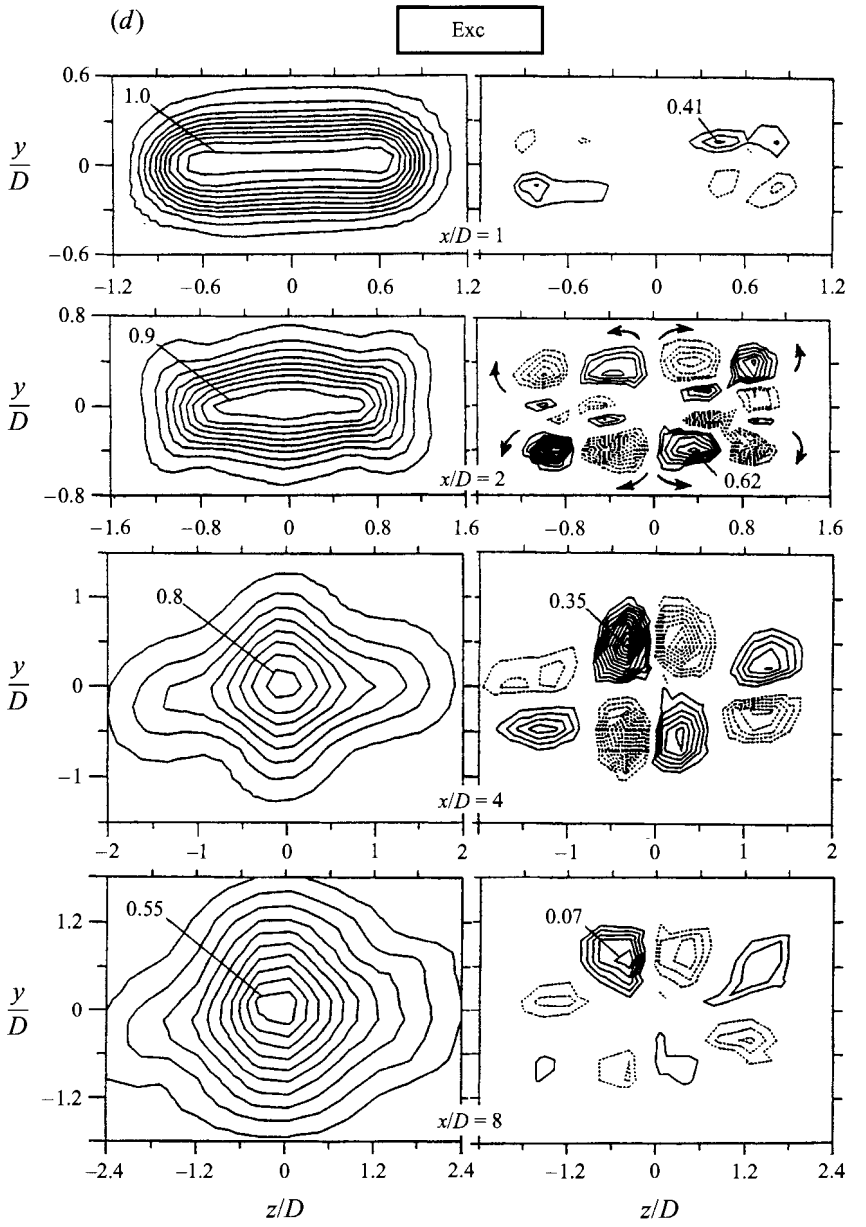

FIGURE 4. Contours of mean velocity (U/U_j, left column) and streamwise vorticity ($\omega_x D/U_j$, right column) for indicated x/D locations; (*a–d*) are for the corresponding tab and excitation cases of figure 3.

in the square nozzle; Quinn 1992.) Nevertheless, the contrast discussed in the preceding paragraph should make it clear that the geometry of the upstream flow path can have an impact on the distribution of the streamwise vortices occurring at the nozzle exit. Such a difference, in the initial ω_x-distribution, can have a profound influence on the subsequent evolution and axis switching of the free jet. This becomes evident from the data for the tab cases shown in figures 4(*b*) and 4(*c*).

Figure 4(*b*) shows data for the case with two delta tabs placed on the narrow edges. For space conservation data only up to $x/D = 8$ are shown for this and the subsequent

cases. The tabs have generated two pairs of streamwise vortices which, as expected (Zaman *et al.* 1994), are of the inflow type. This is opposite to that occurring in the no tab case. The delta tabs have apparently overwhelmed the naturally occurring outflow pairs. However, two additional pairs of the latter sense are seen at $x/D = 2$ and 4. It is not clear, but these could be remnants of the naturally occurring vortices gathering strength because of the contraction of the flow in the direction of the major axis. The inflow vortex pairs produced by the tabs persist far downstream and the accompanying axis switching of the jet can be clearly seen from the mean velocity distributions.

When two delta tabs are placed on the long edges of the nozzle (figure 4*c*), two vortex pairs are introduced in addition to the naturally occurring vortices. Here, the proximity of like-signed vortices induce amalgamation. The amalgamation is complete by $x/D = 8$, where the four pairs have yielded two pairs. The jet cross-section in this case has not only stayed elongated in the major axis plane but has almost bifurcated. (Note that in all the cases of figure 4 a mild anticlockwise turning of the jet cross-section has taken place by the farthest downstream location. This, most likely due to an asymmetry in the recirculating flow within the laboratory, is also consistent with somewhat lower negative levels of ω_x compared to the corresponding positive levels observed at the downstream locations. However, this is inconsequential in the context of the present paper.)

The effect of the excitation on the evolution of the jet is shown in figure 4(*d*). A significant increase in the jet spreading can be observed from the mean velocity contours. This observation is in general agreement with that made by Ho & Gutmark (1987) and by Hussain & Husain (1989). Comparison of the data sets for $x/D = 8$ makes it apparent that the excitation (figure 4*d*) has increased the spreading more than that achieved by the two tab configurations (figures 4*b* and 4*c*). However, there are other tab and nozzle configurations which increase the spreading much more (Zaman 1994). Note that the excitation results in a more complex ω_x-distribution. Two additional pairs of vortices can be seen to emerge in the middle of the jet cross-section, even in these time-averaged data, which were absent closer to the nozzle exit. The additional streamwise vortices occurring farther downstream ($x/D > 2$) must trace their origin to the distortion and reorientation of the azimuthal vortex structures. This issue is addressed further in §3.3.

3.2. *Mechanism of axis switching*

As stated before, Hussain & Husain (1989), in their report of measurements of elliptic jets, provided an explanation for axis switching. This was based on the dynamics of the azimuthal vorticity. Figure 5 is a simplified version of one of their figures included here to help explain these ω_Θ-dynamics. Consider a periodically forced elliptic jet, such as obtained by plane-wave acoustic excitation. Shortly downstream of the nozzle, the azimuthal vorticity rolls up into elliptic vortex rings. One such ring is represented by the structure on the left in figure 5. Owing to the difference in azimuthal curvature, a segment of the ring located at either end of the major axis has higher induced velocity than that of a segment located at either end of the minor axis. Thus, the former segment convects faster. Furthermore, the induced velocity of the segment is directed along its binormal (see the cited reference); thus, the faster moving segment also curls up and protrudes into the core of the jet. The initially elliptic ring, as a result, goes through a sequence of contortions. As represented by the fourth structure from the left, the ring approximately regains its original shape somewhere downstream except that the major and the minor axes are switched. The sequence of events can repeat farther downstream.

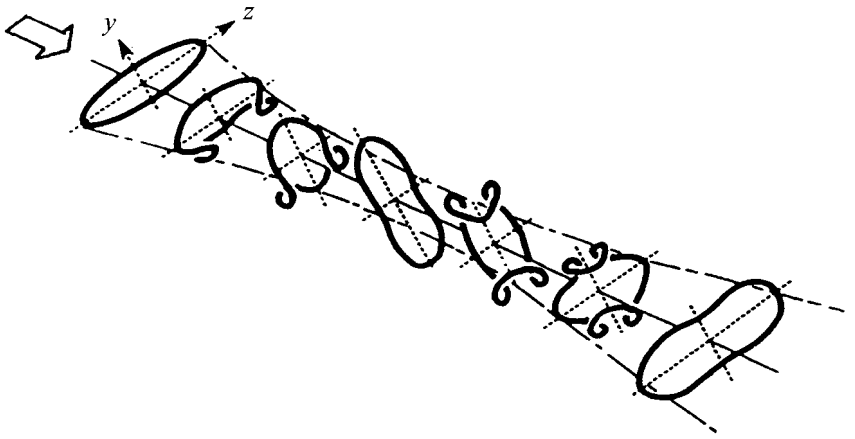

FIGURE 5. The 'ω_θ-dynamics': sequence of deformations of an asymmetric vortex ring leading to axis switchings, from Hussain & Husain (1989).

That such a process occurs with an isolated asymmetric vortex ring had been shown earlier (Kambe & Takao 1971; Viets & Sforza 1972; Dhanak & Bernardinis 1981). Flow-visualization pictures illustrating similar deformations of asymmetric vortex rings, in jets, have been shown by Ho & Gutmark (1987) and Hussain & Husain (1989). In the forced jet, of course, this process occurs periodically. Successive vortex rings go through the same sequence of deformation. However, since the deformation of an individual ring is also a function of streamwise distance, the sequence shown in figure 5 reflects even on the time-averaged flow field, and this leads to the axis switching of the jet.

While the description above is given in terms of a periodically forced jet, the process also occurs in a natural asymmetric jet because there is natural roll-up of the azimuthal vorticity. In the natural jet, however, the formation and subsequent evolution of the vortex rings are more random. The randomness results in a delayed axis switching or simply a transition to round shape without switching of the axes. Conversely, periodic forcing of a natural jet organizes the coherent vortical structures which, by accentuating the ω_θ-dynamics, yields faster axis switching. This is the effect seen in the data of figure 3(*d*) when compared to the data of figure 3(*a*). An earlier axis switching under the influence of acoustic excitation was also observed by Hussain and Husain (1989) for an elliptic jet.

Here, let us refer back to the data of figure 1. The axis switching in the supersonic condition, in contrast to the subsonic condition, was surprising. It was surprising because axis switching was thought to be uncommon with supersonic large-scale jets in various applications. There was also some analytical support, based on stability analysis of elliptic jets, that increasing compressibility reduced the tendency for axis switching (Koshigoe, Tubis & Ho 1988). Yet, all the asymmetric nozzles tested by the author (Zaman 1994) yielded axis switching at supersonic conditions; figures 1(*c*) and 1(*d*) show an example. It is believed that a mechanism similar to that described in the previous paragraph is responsible for the axis switching in these cases. All the jets at the measurement Mach number of $M_j = 1.63$ involved screech (the screech frequency was 6.3 kHz in the case of figures 1*c* and 1*d*). For the purposes of the present discussion, it should suffice to only consider the fact that screech is a self-excitation of supersonic jets which results in the emission of a single tone. It occurs through the interaction of coherent structures with the shock-expansion cells in the flow, and a

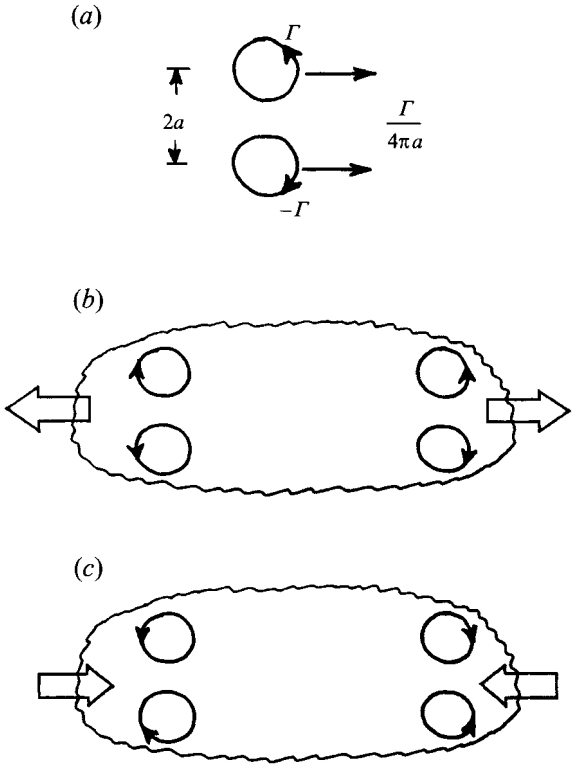

FIGURE 6. The 'ω_x-dynamics': (*a*) induced velocities of a vortex pair, (*b*) distribution of streamwise vortex pairs resisting axis switching, (*c*) distribution promoting axis switching.

completed feedback loop, that organizes the initial vortical structures. Thus, an asymmetric jet with screech is also a periodically forced flow, albeit occurring naturally, in which the faster axis switching is thought to have occurred by accentuated ω_θ-dynamics. (In passing, note by comparison of the data for the two Mach numbers in figure 1 that the jet appears to have spread more in the supersonic condition. However, the normalized mass fluxes, as indicated in the figure caption, show that the increase in the flux has actually been less in the supersonic case; this apparent anomaly is due to higher initial density in the supersonic case. The results on jet entrainment for various nozzles will be reported separately.)

The ω_θ-dynamics, however, do not clearly explain the observations made with the tabs. If it is assumed that the azimuthal vorticity rolls up with an initial shape similar to that determined by the downstream edges of the tabs and the nozzle, it might be possible to explain some of the observed trends. However, the flow fields are more complex for these cases, and the applicability of the ω_θ-dynamics is not straightforward. A much simpler and more satisfactory explanation can be given in terms of the induced velocities of the streamwise vortex pairs. Consider the vortex pair with equal and opposite strength $\pm\Gamma$ and spaced $2a$ apart, as sketched in figure 6(*a*). Recall from vortex dynamics that both the vortices will move to the right with a speed equal to $\Gamma/4\pi a$ (Eskinazi 1967). The fluid between them will also be ejected to the right at about four times this speed. Therefore, the dynamics of the two pairs of streamwise vortices sketched in figure 6(*b*), representative of the natural jet case (figure 4*a*), would tend to elongate the jet cross-section in the direction of the major axis. Conversely, for the distribution sketched in figure 6(*c*), representative of the tab case of figure 4(*b*), both

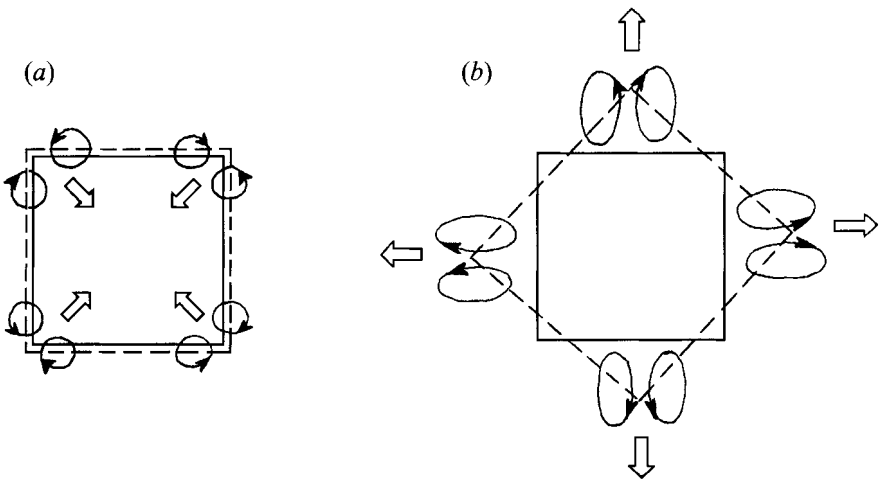

FIGURE 7. Schematic of mean streamwise vorticity distributions in a square jet, after the results of Quinn (1992): (*a*) distribution close to the jet exit, (*b*) distribution farther downstream.

pairs would move towards the jet centreline. This would result in a contraction of the jet cross-section in the direction of the major axis.

It should follow, therefore, that the ω_x-dynamics described in the foregoing would resist axis switching in the natural jet case of figure 4(*a*). On the other hand, axis switching would be promoted in the tab case of figure 4(*b*). These are indeed the observed trends. Note that in the cases of figures 4(*b*) and 6(*c*), once the two pairs of vortices have moved close to each other, the new pairs formed above and below the major axis would then move away from the jet axis. The vortex distribution in this case, therefore, supports an efficient mechanism causing the *first* axis switchover. *It should be clear that the ω_x-dynamics will not support further axis switchings beyond the first.* Possible further switchings may occur only through the ω_Θ-dynamics. It should also be easy to see that the motions of the vortex pairs in the case of figure 4(*c*) are similar to those in the natural jet case (figure 4*a*), i.e. all four pairs move away from the jet centreline in the direction of the major axis. The jet cross-section thus elongates in that direction. In fact, owing to the additional vortices, the pull is so much that the jet cross-section is essentially bifurcated.

The ω_x-dynamics can also explain the 45° axis switching observed in the square jet experiment of Quinn (1992). Quinn's measurements showed four inflow pairs of vortices occurring close to the nozzle exit at $x/D = 0.28$, as sketched in figure 7(*a*). It is not completely clear, but the origin of these vortices is also thought to be upstream secondary flow as in Davis & Gessner's (1992) experiment. With the given vorticity distribution, in any case, it should be easy to see that each vortex pair at first moves towards the jet centreline. Two vortices on a side then form an outflow pair. The four resulting pairs then move away from the jet centreline, as sketched in figure 7(*b*), causing the 45° switching of the axes.

A similar 45° axis switching has also been observed with a periodically forced square jet in the computational study of Grinstein (1993). In the computation, however, there is no streamwise vorticity initially. Thus, the 45° switching in that flow must have occurred due to the dynamics of the azimuthal vorticity. The azimuthal vorticity initially rolls-up into a square ring. The corners of the ring then deform and reorient in a manner similar to that described with figure 5, and this eventually results in the 45° axis switching. The 'volume visualization' of vorticity presented by Grinstein provides

an insight into these processes (see also Grinstein *et al.* 1994). The axis switchings observed by Toyoda *et al.* (1991), with orifice jets of various cross-sections, apparently also occurred due to the ω_Θ-dynamics.

It is likely that a combination of the ω_Θ- and ω_x-dynamics may also explain the difference in the behaviour of jets from 'slot nozzles' with and without an upstream contraction (Gutmark & Schadow 1987). In the case without the contraction, it is likely that the former dynamics played the dominant role to cause the axis switching. In this case, there is no nozzle wall upstream where the boundary layer could be subjected to lateral pressure gradient; thus, the source of ω_x is essentially absent. With the addition of the upstream contraction, the flow field could be similar to that in the present natural jet (no tab, no excitation case, figure 4*a*). The likely presence of outflow vortex pairs could have, like the present case, resisted the axis switching.

It should be quite apparent by now that the ω_Θ- and ω_x-dynamics may not be independent of each other. The streamwise vortices are embedded in a sheet of azimuthal vorticity. Thus, the ω_x-dynamics are influenced by the forces exerted by the latter vorticity field. Conversely, the reorientation of the azimuthal vorticity gives rise to streamwise vortex pairs the influence of which constitutes an integral part of the ω_Θ-dynamics. The following experiment was conducted in an effort to gain further insight into these complex processes.

3.3. *Phase-averaged vorticity field for the excitation case*

Corresponding to the excited case of figures 3(*d*) and 4(*d*), detailed phase-averaged flow field measurements were carried out. The underlying concepts and the procedure were the same as in Hussain & Zaman (1980). The excitation signal was used as reference. The same probe arrangement as described in §2 was used. The four hot-wire signals and the reference signal were sampled simultaneously. The phase averaging was performed on-line using the peaks in the reference signal as triggers. The $\langle u\rangle$, $\langle v\rangle$ and $\langle w\rangle$ data for 19 phases, within a period, were stored for each of the grid points on a (y, z)-plane. As done with the time-averaged data, gradient corrections for $\langle v\rangle$ and $\langle w\rangle$ were performed based on the $\langle u\rangle$ gradients, and the $\langle w\rangle$-array was shifted to match the $\langle v\rangle$-array. These data were post processed to obtain streamwise vorticity, $\langle\omega_x\rangle = \partial\langle w\rangle/\partial y - \partial\langle v\rangle/\partial z$.

The components $\langle\omega_y\rangle$ and $\langle\omega_z\rangle$ were estimated invoking the Taylor hypothesis as $\langle\omega_y\rangle = \partial\langle u\rangle/\partial z + (1/U_c)\partial\langle w\rangle/\partial t$, and $\langle\omega_z\rangle = -(1/U_c)\partial\langle v\rangle/\partial t - \partial\langle u\rangle/\partial y$. Here, the notation t represents time with respect to a trigger location, and U_c is a convection velocity. From the two azimuthal components of vorticity the quantity $\langle\xi\rangle = (\langle\omega_y\rangle^2 + \langle\omega_z\rangle^2)^{1/2}$ was calculated which approximated enstrophy. Its significance is described further in the following. In applying the Taylor hypothesis, $U_c = 0.5U_j$ was assumed. It should be noted that the latter assumption was shown by Zaman & Hussain (1981) to work reasonably well for the eduction of non-interacting large-scale vortical structures. The vortical structures in the present flow, however, involve rapid evolution, which is a situation where the applicability of Taylor hypothesis may be questionable (see also LeBoeuf & Mehta 1995). Because of this and the hot-wire errors discussed in §2, the $\langle\xi\rangle$ data should be considered as only qualitative estimates. The distributions of $\langle\omega_x\rangle(y, z, t)$ and $\langle\xi\rangle(y, z, t)$ were obtained at a number of streamwise locations. From these data spatial distributions of these properties were also constructed over a volume of the flow field for a given phase.

Since the excitation signal at the fundamental frequency was used as reference in the phase averaging, it was necessary to ensure that the flow field did not develop a subharmonic, e.g. through vortex pairing. The phase averaging would otherwise

provide a 'double image' of the actual coherent structures. Thus, a hot-wire survey was first conducted. The u'-spectra measured on the jet centreline are shown in figure 8(*a*); the traces are for the indicated x/D locations and successive ones are staggered by one major ordinate division. The abscissa is linear and the ordinate is logarithmic but arbitrary; the amplitude variations for the spectral components are shown in figure 8(*b*). At $x/D = 0$ in figure 8(*a*), the fundamental dominates the spectrum. Line noise at 60 Hz and its harmonics are seen at lower frequencies but these are inconsequential to the flow field. With increasing x/D the fundamental grows and at $x/D = 1$ a subharmonic appears. The growth and decay of the fundamental and the subharmonic farther downstream are essentially similar to those observed previously with circular jets (e.g. by Crow & Champagne 1971, and Zaman & Hussain 1980). The maximum level of about 9% (figure 8*b*), and the location of $x/D \approx 1.5$ where the fundamental reaches it, for $St = 0.6$, were essentially the same with a circular jet.

The subharmonic amplitude was less than one third of the fundamental amplitude upstream of $x/D = 2.2$. This was deemed sufficiently small and thus $x/D = 2.2$ was chosen as the downstream limit for the phase-average measurements. Cursory surveys at off-axis locations showed that the subharmonic was substantially smaller everywhere up to this x/D. As stated in §2, probe resolution considerations set the upstream limit for these measurements at $x/D = 0.85$. Referring back to figure 3(*d*), note that the chosen region for the phase-averaged measurements is upstream of the axis switchover location. (As the spectral peaks disappear underneath broadband turbulence shortly downstream of $x/D \approx 4$, the phase averaging would not be meaningful around and beyond that location anyway.) Thus, the data presented in the following captures the details of the flow field prior to and leading to the axis switchover.

The phase variation for the fundamental corresponding to the data of figures 8(*a*) and 8(*b*) is shown in figure 8(*c*). The phase data yield a wavelength of approximately $\lambda/D = 1$, within $x/D = 2.2$. This corresponds to a convection velocity $U_c/U_j = 0.6$. However, the convection velocity of coherent structures is somewhat overestimated when measured on the jet centreline, thus $U_c = 0.5U_j$ has been used with the Taylor hypothesis based on past experience (Zaman & Hussain 1981).

The distributions of $\langle\omega_x\rangle$, on a cross-sectional plane of the jet at $x/D = 2$, are shown in figure 9 for four phases (ϕ), as examples. The phases are chosen approximately at equal intervals within the period. Note that the time-averaged ω_x distribution corresponding to these data were shown in figure 4(*d*). The data in figure 9 show that the streamwise vorticity distribution goes through dramatic changes with time (i.e. phase) within a period. Compare, for example, the data for $\phi = 0°$ and 176°. The dominant vortex pairs in the two plots are of opposite sense! These data underscore the fact that the vorticity dynamics are much more vigorous than what is revealed by the time-averaged flow field. In a flow downstream of a 'delta tab', Bohl & Foss (1994) have measured the r.m.s. of ω_x to be as much as six times larger than the corresponding mean amplitude. In the present flow, the time-averaged ω_x near the jet exit is of small magnitude ($x/D = 1$, figure 4*d*), but the amplitudes are seen to actually increase farther downstream. The appearance of larger amplitude ω_x farther downstream, as well as the reversals in the $\langle\omega_x\rangle$ distributions in figure 9, can be traced to a reorientation of the azimuthal vorticity. This becomes clear with the following data.

Figure 10 shows the time variation of an isosurface of $\langle\xi\rangle$, on the (y, z)-plane at $x/D = 2$. The variation includes all 19 phase points approximately covering the full period. Since the magnitude of either $\langle\omega_y\rangle$ or $\langle\omega_z\rangle$ is significantly larger than that of $\langle\omega_x\rangle$, $\langle\xi\rangle$ closely approximates enstrophy, the true value of which would also include contribution from $\langle\omega_x\rangle$. With an appropriate choice of the isosurface level, $\langle\xi\rangle$

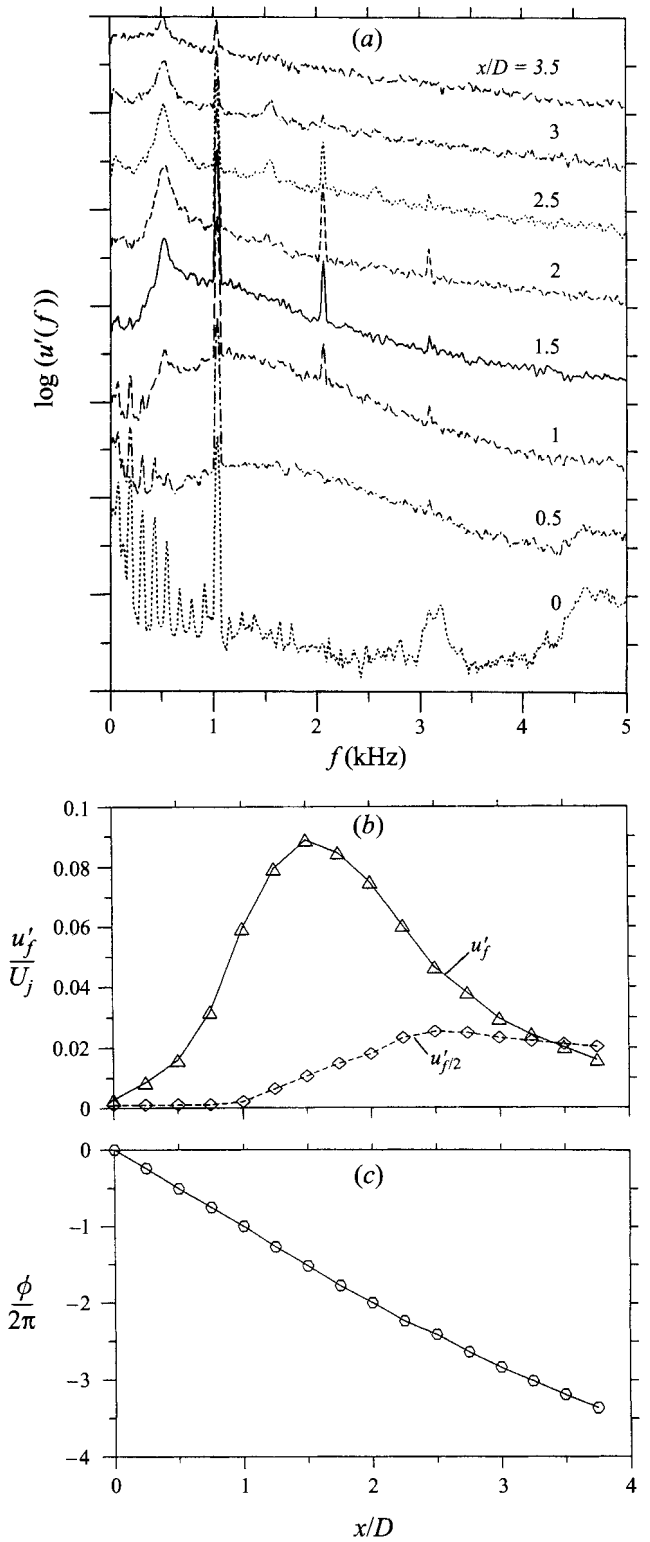

FIGURE 8. Evolution of velocity spectra on the jet centreline for the excited case. (*a*) u'-spectra at indicated x/D. (*b*) Amplitude variations for fundamental and subharmonic. (*c*) Phase variation for the fundamental.

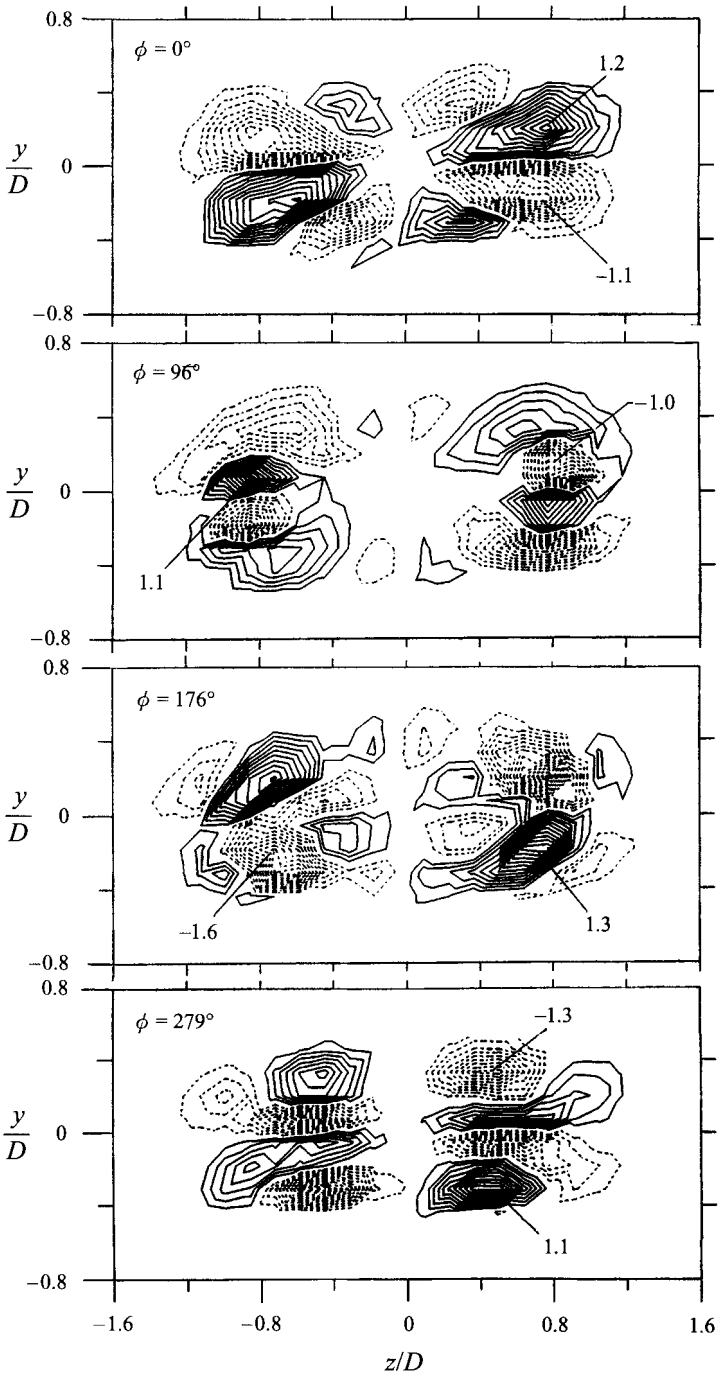

FIGURE 9. Contours of phase-averaged streamwise vorticity, $\langle \omega_x \rangle D/U_j$, measured at $x/D = 2$ for the excitation case. The four sets of data are for indicated phases (ϕ).

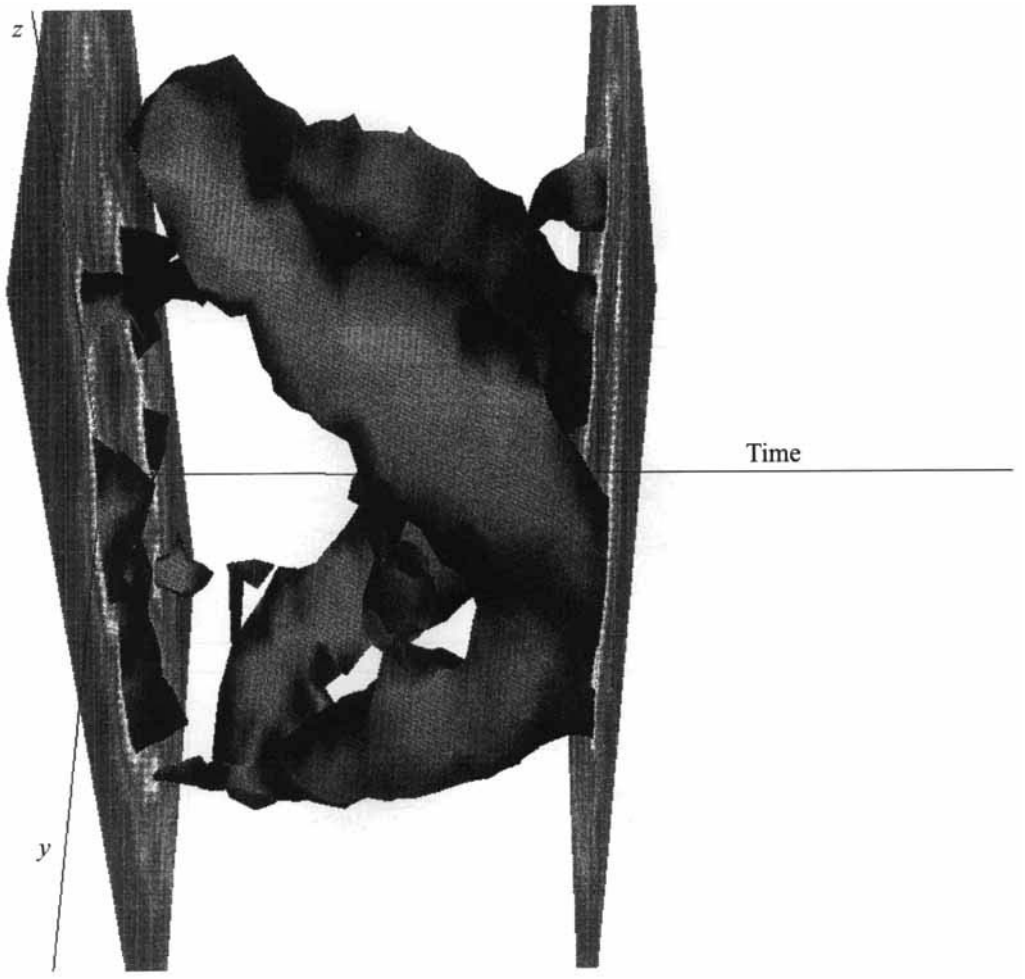

FIGURE 10. Temporal distribution of an isosurface of enstrophy, $\langle\xi\rangle D/U_j = 2.7$, measured at $x/D = 2.0$, shown over a complete period of the excitation.

provides an indication of the concentration of the azimuthal vorticity within the flow field. Inspection of figure 10 reveals the presence of a distorted vortex ring. The azimuthal vorticity which initially rolls up into an approximately elliptic shaped vortex ring has gone through a contortion by $x/D = 2$, in a manner similar to that described with figure 5. Note that positive time corresponds to negative x, and thus the distortion appears reversed. To the author's knowledge, this is a first set of experimental data quantitatively confirming such distortion seen earlier mainly by flow visualization (Ho & Gutmark 1987; Hussain & Husain 1989).

The spatial distributions of $\langle\xi\rangle$ over the full volume of the flow field are shown in figure 11. While figure 10 showed temporal distribution at a fixed x/D, each set of data in figure 11 represents spatial distribution for a fixed phase. The four data sets correspond to the same four phases of figure 9. For display purposes the x-coordinate has been stretched by a factor of 2 and the origin is shown at $x/D = 0.5$ instead of at $x/D = 0$; i.e. $x' = 2(x - 0.5D)$. The data cover the region from $x/D = 0.85$ to 2.2. Also, since the magnitude of $\langle\xi\rangle$ decreases substantially with increasing x, the choice of a level for the isosurface enabling a visualization of the whole flow field was difficult. A small level would mask the details of the coherent structures while a large level would

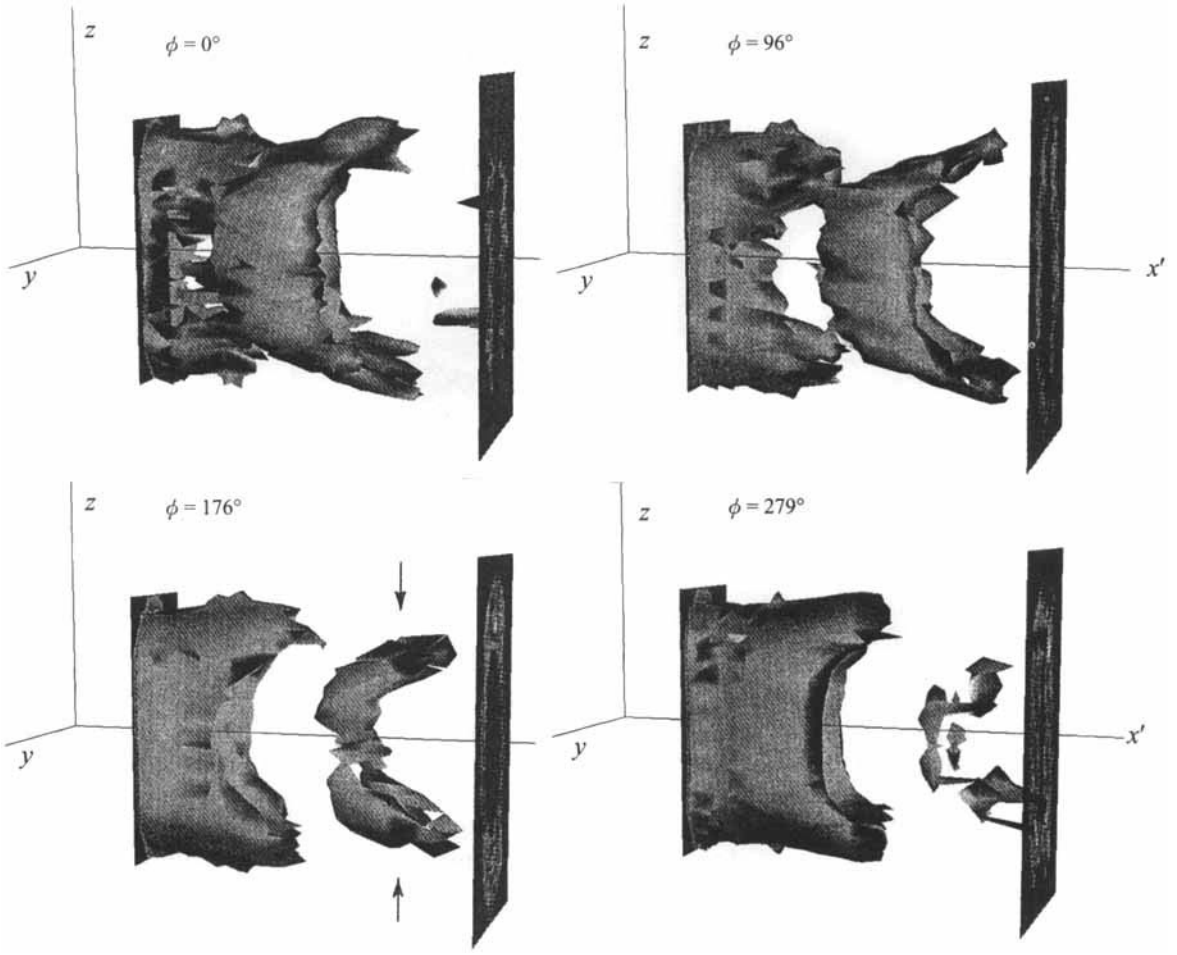

FIGURE 11. Spatial distributions of an isosurface of enstrophy, $\langle \xi \rangle D/U_j = 3.2$, for the four phases of figure 9.

show them only at the upstream locations. The level indicated in the figure caption was chosen after some trial.

The evolution of the azimuthal vorticity field with time is captured by the data in figure 11. The sheet of azimuthal vorticity emerging from the nozzle can be seen to form isolated structures. Such a structure is about to break off in the data set for $\phi = 0°$. The segments at the ends of the major axis are already tilted forward. These apparently become more tilted as the structure propagates downstream. It should be apparent that such deformations contribute to the x-component of vorticity which is further illustrated in the following.

The temporal distributions of $\langle \omega_x \rangle$ corresponding to the data of figure 10 are shown in figure 12. Two views, approximately projecting on the major and the minor axis planes, are shown. Since $\langle \omega_x \rangle$ involves negative and positive amplitudes, two iso-surfaces are required to show these variations. The data provide a comprehensive picture of the $\langle \omega_x \rangle$ field. At a given instant the (y, z)-plane contains two streamwise vortex pairs. These two pairs are of a certain sense (inflow or outflow). Approximately one half-period away, as was seen in figure 9, the same (y, z)-plane contains two pairs with an opposite sense.

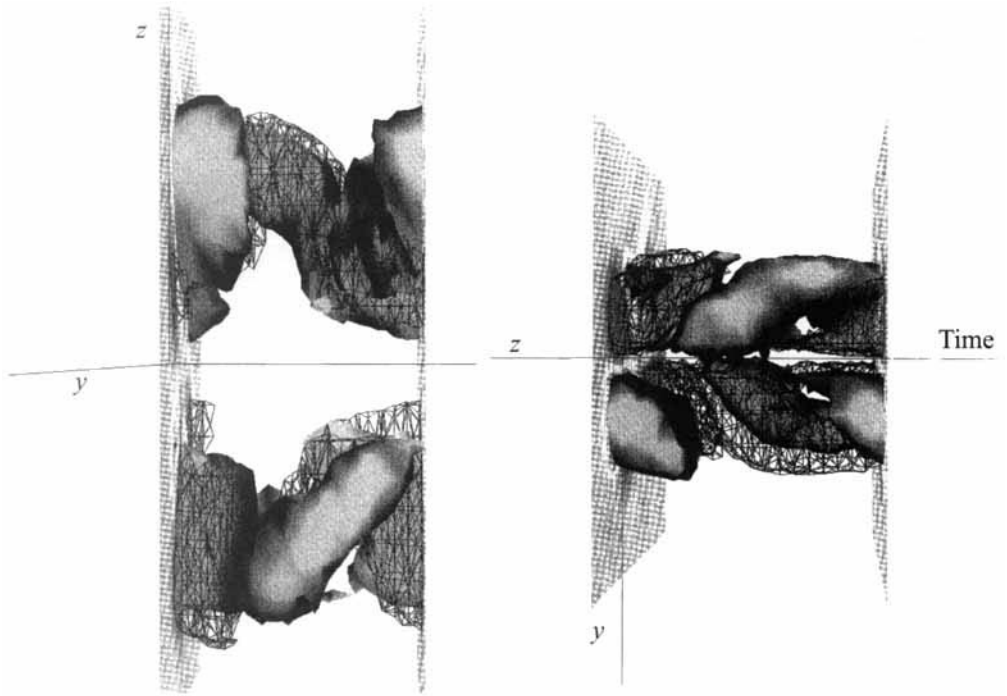

FIGURE 12. Temporal distributions of two isosurfaces of streamwise vorticity, $\langle\omega_x\rangle D/U_j = 0.3$ (solid) and -0.3 (transparent net-like), measured at $x/D = 2$. The two images are two views of the same set of data.

A clearer idea of the sense of rotation of the streamwise vortex pairs is obtained from the spatial distributions of $\langle\omega_x\rangle$. Such distributions, corresponding to the four phases of figure 11, are shown in figure 13. Clearly, the flow field at a given phase is characterized by two pairs of streamwise vortices which alternate in sense with varying x. Now let us consider the two vortex pairs marked by the vertical arrows in the data set for $\phi = 176°$. The same locations in the corresponding data set of figure 11 are also marked by two vertical arrows. If the isolated vortex structure in figure 11 at this location is considered, it should not be difficult to see that the tilting of the narrow ends of the structure must generate two inflow pairs of streamwise vortices. These are the two pairs seen in figure 13 at the corresponding arrow locations. The two preceding vortex pairs in figure 13, marked by the inclined arrows, have the outflow sense of rotation. The deformation of an azimuthal vortex ring, as seen in figures 10 and 11, however, cannot produce streamwise vortex pairs with this sense. There where are these arising from?

The answer most likely can be traced to another feature of the vorticity field that has not been addressed so far. Referring back to figure 4, one might wonder what happened to the streamwise vortices, originating from secondary flow within the nozzle, seen in (*a*), when the periodic excitation was applied, in (*d*). It is unlikely that the excitation has appreciably changed the flow field within the nozzle. Excitation, with comparable amplitudes, has been known not to alter even the boundary layer state at the nozzle exit (Zaman & Hussain 1980). The source of the streamwise vortices (Prandtl's first kind of secondary flow) must, therefore, be present even under the excitation. It is apparent that the outflow pairs of vortices originating from this source have been redistributed by the excitation. The excitation has lumped this vorticity

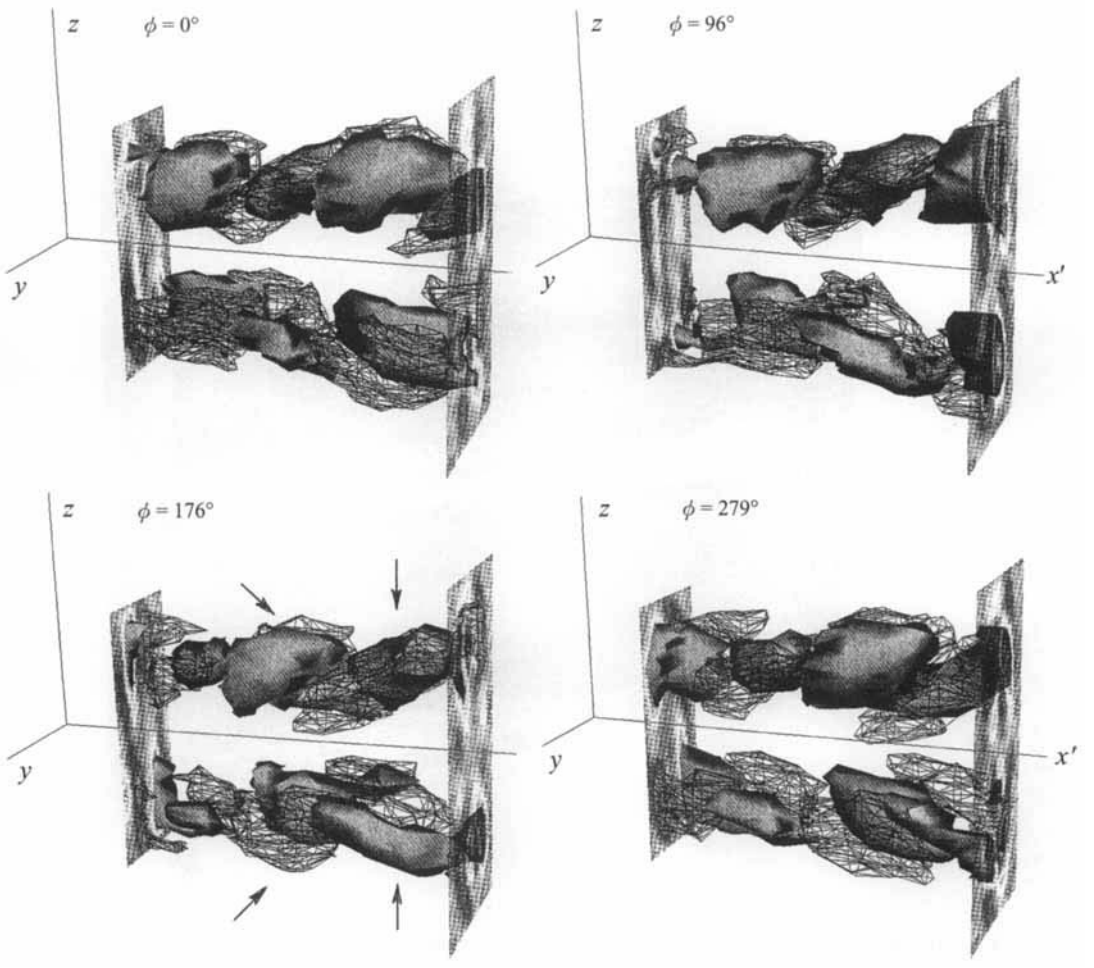

FIGURE 13. Spatial distributions of isosurfaces of streamwise vorticity, $\langle \omega_x \rangle D/U_j = \pm 0.3$, for the four phases of figures 9 and 11.

periodically in space. It is thought that this is how the vortex pairs marked by the inclined arrows in figure 13 have appeared. Thus, on either side of the minor axis plane, an inflow pair generated by the reorientation of ω_θ is followed by an outflow pair that traces its origin to secondary flow within the nozzle. The sequence is repeated with the passage of each vortical structure.

Finally, figure 14 shows the distribution of time-averaged ω_x over the measurement volume. This distribution may be compared with the phase-averaged data of figure 13. It should be apparent from the choice of the isosurface levels that the time-averaged amplitudes, as expected, are much smaller than the corresponding phase-averaged amplitudes. The time-averaged streamwise vortices have resulted from a combination of contributions from the nozzle secondary flow and the distortion of azimuthal vorticity. The distribution is complex, as was also indicated by the data of figure 4(*d*), and involves several vortex pairs. Towards the downstream end of the measurement volume four pairs of vortices can be identified. The outer two pairs are of the outflow sense and must be mainly due to the nozzle secondary flow. The inner two pairs, of the inflow sense, must be mainly due to the deformation of the azimuthal vortex rings. It is remarkable that out of the vigorous time-dependent activity these distinct vortex

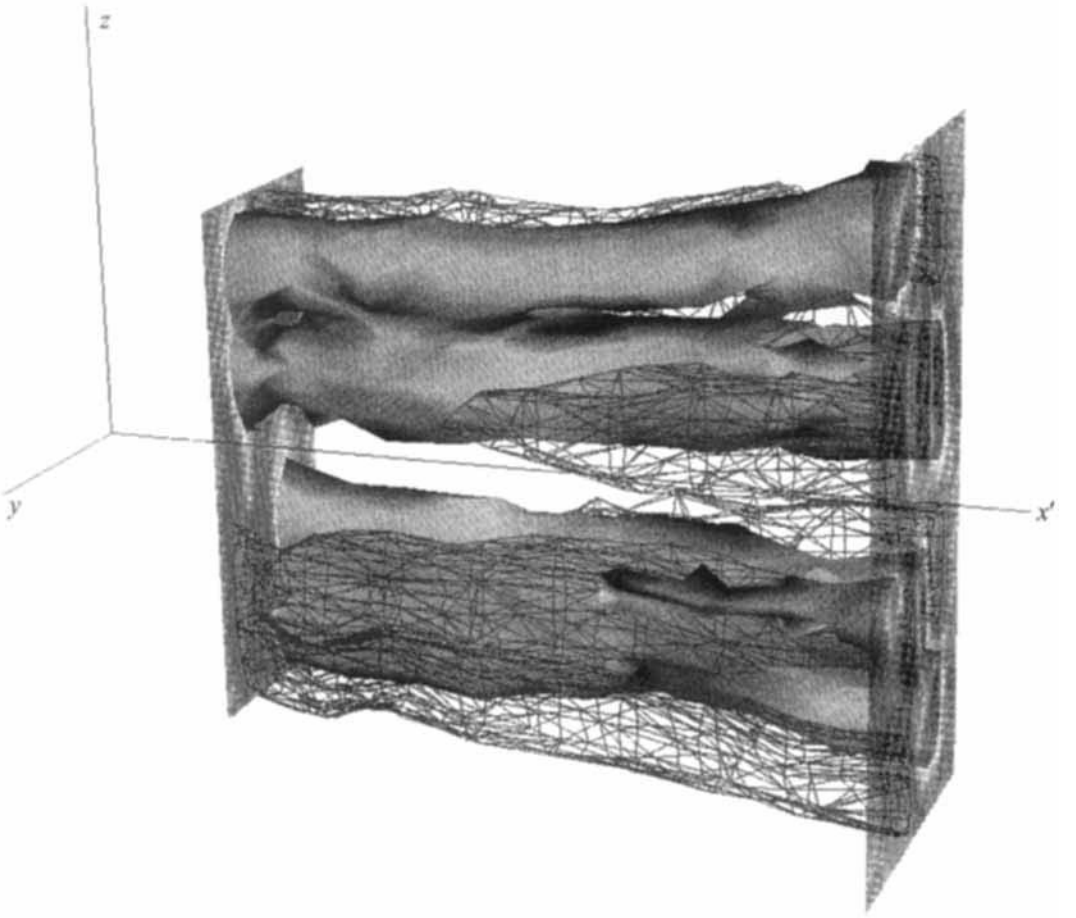

FIGURE 14. Spatial distribution of time-averaged streamwise vorticity, $\omega_x D/U_j = \pm 0.11$.

pairs emerge in the time-averaged flow field. The ω_x-dynamics associated with the four pairs are also consistent with the characteristic deformation of the jet cross-section observed at the downstream locations of figure 4(*d*).

4. Concluding remarks

In this paper the results of an experimental study on a free rectangular jet have been presented. Vortex generators in the form of tabs are used to introduce streamwise vortices and periodic excitation is used to organize the azimuthal coherent structures. Both of these affect the phenomenon of axis switching and thus provide insight into the underlying mechanisms.

The basic flow, without excitation or vortex generators, is characterized by four streamwise vortices which trace their origin to secondary flow within the nozzle. These form two counter-rotating pairs located on each end of the major axis. These are of the outflow type, i.e. with a sense of rotation so as to eject jet core fluid into the ambient. These vortices fade away by $x/D = 16$, and the jet has not gone through an axis switching by that distance. The use of two delta tabs, placed on the narrow edges of the nozzle, cause changes in the flow upstream to produce two opposite, inflow pairs. The jet in this case goes through a rapid axis switching. Two delta tabs placed on the

long edges of the nozzle, on the other hand, produce vortex pairs with sense similar to those existing in the natural case. The like-signed vortices amalgamate and the jet continues to diverge on the major axis plane within the measurement range.

Two mechanisms are identified for the axis switching. One, addressed previously by others, is due to the deformation and reorientation of rolled-up azimuthal vortices. This mechanism, referred to as the ω_θ-dynamics, always tends to cause axis switching. As the azimuthal coherent structures evolve and persist in the flow, this dynamics continues to act causing a second or even a third axis switching. However, randomness dilutes the effect and the latter switchovers are usually not clearly detectable. Randomness also affects the first switchover and causes its location to shift downstream. Conversely, when a jet is forced periodically, which organizes the azimuthal coherent structures and removes some of the randomness, it causes the first switchover to occur farther upstream. This has been readily demonstrated in previous, and in the present, experiments by periodic excitation. This is also thought to be the mechanism causing a faster axis switching in screeching supersonic jets, as screech is also a periodic excitation which accentuates the ω_θ-dynamics.

The second mechanism, identified in this study and referred to as the ω_x-dynamics, is due to induced velocities of streamwise vortex pairs. Two pairs of streamwise vortices, situated at the ends of the major axis and having the outflow sense, resist axis switching. Such vortex pairs are often present in jets owing to secondary flow within the nozzle, especially when the nozzle involves round-to-asymmetric contraction sections. Thus, in such jets axis switching is either delayed or may not occur. On the other hand, if two inflow vortex pairs are situated at the ends of the major axis the effects of the ω_θ- and the ω_x-dynamics supplement each other and cause a rapid axis switching. This was the case when two tabs were located on the narrow edges of the nozzle. Conversely, when two tabs were located on the long edges, the outflow vortex pairs were reinforced to provide additional resistance to axis switching.

Thus, cancelling effects between the ω_θ- and ω_x-dynamics are thought to be responsible for the slow or no axis switching occurring with many asymmetric nozzles. With asymmetric orifices, on the other hand, a rapid axis switching is due to the dominance of the ω_θ-dynamics. Since there is no significant upstream secondary flow to produce streamwise vortices the opposing effect of ω_x-dynamics is absent in this case. Either the ω_x- or ω_θ-dynamics can also explain a 45° axis switching observed with square jets.

The two dynamics are obviously not independent of each other. The streamwise vortices are embedded in a sheet of azimuthal vorticity. Thus, the induced velocities of the latter vorticity field affect the ω_x-dynamics. On the other hand, the reorientation of the azimuthal vorticity generates streamwise vortex pairs. The induced velocities of such vortex pairs become an integral part of the ω_θ-dynamics. In fact, the observed reorientation of an azimuthal vortex produces streamwise vortex pairs with the inflow sense. These vortex pairs augment the effect of the ω_θ-dynamics, contributing to a faster axis switching.

For a periodically forced jet, a detailed set of phase-averaged data are presented in this paper. For a volume of the near flow field, the data show the distribution of the streamwise vortices as well as the azimuthal vortical structures. Data for different phases capture the time variation of these structures. The reorientation of an azimuthal vortex structure, previously seen in flow visualization and computational studies, is demonstrated by these data.

The periodic excitation is observed to alter even the time-averaged streamwise vorticity distribution. At about two equivalent diameters downstream, while the

natural flow contains only two outflow pairs, the excitation results in four pairs. An examination determines that the outer two of these four pairs can be traced to the nozzle secondary flow while the inner two originate from the reorientation of the azimuthal vorticity. The outflow streamwise vortex pairs, due to secondary flow within the nozzle, become redistributed by the excitation. These vortex pairs become periodically lumped in space, with the intervening regions containing vortex pairs of opposite sense occurring from the reorientation of azimuthal vorticity. Thus, the time variation at a given location exhibits vortex pairs of alternating sense. The phase-averaged flow field, therefore, is characterized by much more vigorous vortical activity than that revealed by the time-averaged flow field.

The author is grateful to Dr Judith K. Foss for a careful review of the manuscript.

REFERENCES

AHUJA, K. K. & BROWN, W. H. 1989 Shear flow control by mechanical tabs. *AIAA Paper* 89–0994.

BELL, J. H. & MEHTA, R. D. 1992 Measurements of the streamwise vortical structures in a plane mixing layer. *J. Fluid Mech.* **239**, 213–248.

BOHL, D. G. & FOSS, J. F. 1994 Streamwise vorticity and velocity measurements in the near field of a tabbed jet. *Turbulence in Complex Flows. ASME Winter Annual Meeting*, FED Vol. 203.

BRADSHAW, P. 1987 Turbulent secondary flows. *Ann. Rev. Fluid Mech.* **19**, 53–72.

CROW, S. C. & CHAMPAGNE, F. H. 1971 Orderly structures in jet turbulence. *J. Fluid Mech.* **48**, 547–591.

DAVIS, D. O. & GESSNER, F. B. 1992 Experimental investigation of turbulent flow through a circular-to-rectangular transition duct. *AIAA J.* **30**, 367–375.

DHANAK, M. R. & BERNARDINIS, B. D. 1981 The evolution of an elliptic vortex ring. *J. Fluid Mech.* **109**, 189–216.

ESKINAZI, S. 1967 *Vector Mechanics of Fluids and Magnetofluids*. Academic.

GRINSTEIN, F. F. 1993 Vorticity dynamics in spatially-developing rectangular jets. *AIAA Paper* 93–3286.

GRINSTEIN, F. F., GUTMARK, E. & PARR, T. 1994 Numerical and experimental study of the near field of subsonic, free square jets. *AIAA Paper* 94-0660.

GUTMARK, E. & SCHADOW, K. C. 1987 Flow characteristics of orifice and tapered jets. *Phys. Fluids* **30**, 3448–3454.

HERTZBERG, J. R. & HO, C.-M. 1992 Time-averaged, three-dimensional flow in a rectangular sudden expansion. *AIAA J.* **30**, 2420–2425.

HO, C.-M. & GUTMARK, E. 1987 Vortex induction and mass entrainment in a small-aspect-ratio elliptic jet. *J. Fluid Mech.* **179**, 383–405.

HUSSAIN, F. & HUSAIN, H. S. 1989 Elliptic jets. Part 1. Characteristics of unexcited and excited jets. *J. Fluid Mech.* **208**, 257–320.

HUSSAIN, A. K. M. F. & ZAMAN, K. B. M. Q. 1980 Vortex pairing in a circular jet under controlled excitation. Part 2. Coherent structure dynamics. *J. Fluid Mech.* **101**, 493–544.

LEBOEUF, R. L. & MEHTA, R. D. 1995 On using Taylor's hypothesis for three-dimensional mixing layers, *Phys. Fluids* **7**, 1516–1518.

LIEPMANN, D. & GHARIB, M. 1992 The role of streamwise vorticity in the near-field entrainment of round jets. *J. Fluid Mech.* **245**, 643–668.

KAMBE, T. & TAKAO, T. 1971 Motion of distorted vortex rings. *J. Phys. Soc. Japan* **31**, 591–599.

KIYA, M., ISHII, H. & KITAMURA, M. 1991 Simulating deformation of non-circular vortex rings. *ASME Forum on Turbulent Flows*. FED Vol. 112, pp. 115–120.

KOSHIGOE, S., TUBIS, A. & HO, C.-M. 1988 Vortex deformation in elliptic-core jets from the perspective of linear instability analysis. *Phys. Fluids* **31**, 2504–2517.

KROTHAPALLI, A., BAGANOFF, D. & KARAMCHETI, K. 1981 On the mixing of rectangular jet. *J. Fluid Mech.* **107**, 201–220.

MIAU, J. J., LEU, T. S., CHOU, J. H., LIN, S. A. & LIN, C. K. 1990 Flow distortion in a circular-to-rectangular transition duct. *AIAA J.* **28**, 1447–1456.

QUINN, W. R. 1992 Streamwise evolution of a square jet cross section. *AIAA J.* **30**, 2852–2857.

RAMAN, G., ZAMAN, K. B. M. Q. & RICE, E. J. 1989 Initial turbulence effect on jet evolution with and without tonal excitation. *Phys. Fluids* A **1**, 1240–1248.

SFEIR, A. A. 1976 Investigation of three-dimensional turbulent rectangular jets. *AIAA Paper* 78–1185.

SFORZ, M. P., STEIGER, H. M. & TRENTACOSTE, N. 1966 Studies on three-dimensional viscous jets. *AIAA J.* **4**, 800–806.

SOTIROPOULOS, F. & PATEL, V. C. 1993 Numerical calculation of turbulent flow through a circular-to-rectangular transition duct using advanced turbulence closures. *AIAA Paper* 93-3030.

TOYODA, K., SHIRAHAMA, Y. & KOTANI, K. 1991 Manipulation of vortical structures in noncircular jets. *ASME Forum on Turbulent Flows.* FED Vol. 112, pp. 125–140.

TRENTACOSTE, N. & SFORZA, P. 1967 Further experimental results for three-dimensional free jets. *AIAA J.* **5**, 885–891.

TSUCHIYA, Y., HORIKOSHI, C. & SATO, T. 1986 On the spread of rectangular jets. *Exps. Fluids* **4**, 197–204.

VIETS, H. & SFORZA, P. M. 1972 Dynamics of bilaterally symmetric vortex rings. *Phys. Fluid* **15**, 230–240.

ZAMAN, K. B. M. Q. 1994 Effect of 'delta tabs' on mixing and axis switching in jets from asymmetric nozzles. *AIAA Paper* 94-0186.

ZAMAN, K. B. M. Q. & HUSSAIN, A. K. M. F. 1980 Vortex pairing in a circular jet under controlled excitation. Part 1. General jet response. *J. Fluid Mech.* **101**, 449–491.

ZAMAN, K. B. M. W. & HUSSAIN, A. K. M. F. 1981 Taylor hypothesis and large-scale coherent structures. *J. Fluid Mech.* **112**, 379–396.

ZAMAN, K. B. M. Q., REEDER, M. F. & SAMIMY, M. 1994 Control of an axisymmetric jet using vortex generators. *Phys. Fluid* A **6**, 778–793.